Magnetic hysteresis behavior and magnetic pinning in a d(0) ferromagnet/superconductor nanostructure

Uchino, Takashi
Uenaka, Yuki
Soma, Haruka
Sakurai, Takahiro
Ohta, Hitoshi

(Citation)
Journal of Applied Physics,115(6):063910-063910

(Issue Date)
2014-02-14

(Resource Type)
journal article

(Version)
Version of Record

Magnetic hysteresis behavior and magnetic pinning in a d 0 ferromagnet/superconductor nanostructure

Takashi Uchino, Yuki Uenaka, Haruka Soma, Takahiro Sakurai, and Hitoshi Ohta

Citation: Journal of Applied Physics **115**, 063910 (2014); doi: 10.1063/1.4865876
View online: http://dx.doi.org/10.1063/1.4865876
View Table of Contents: http://scitation.aip.org/content/aip/journal/jap/115/6?ver=pdfcov
Published by the AIP Publishing

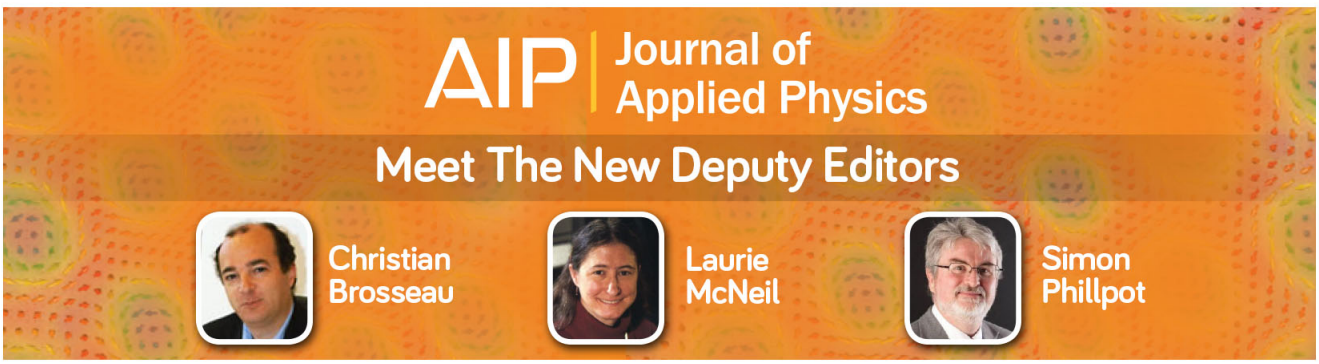

Magnetic hysteresis behavior and magnetic pinning in a d^0 ferromagnet/superconductor nanostructure

Takashi Uchino,[1,a)] Yuki Uenaka,[1] Haruka Soma,[1] Takahiro Sakurai,[2] and Hitoshi Ohta[3]
[1]*Department of Chemistry, Graduate School of Science, Kobe University, Nada, Kobe 657-8501, Japan*
[2]*Center for Support to Research and Education Activities, Kobe University, Nada, Kobe 657-8501, Japan*
[3]*Molecular Photoscience Research Center and Graduate School of Science, Kobe University, Nada, Kobe 657-8501, Japan*

(Received 24 September 2013; accepted 3 February 2014; published online 14 February 2014)

We investigate the interaction between superconductivity and defect-induced d^0 ferromagnetism using a composite consisting of MgB_2 and MgO nanocrystals. The composite exhibits a ferromagnetic hysteresis behavior in the temperature region from 40 to 300 K. Defective MgO nanocrystals (~20 nm) embedded in the composite are considered to be responsible for the observed ferromagnetism. The zero field cool and field cool magnetization curves show that the superconducting transition occurs at $T_c = 38.6$ K, in agreement with T_c of pure MgB_2. In the temperature region from T_c to $0.9T_c$ (~35 K), the magnetization hysteresis curves show a superposition of ferromagnetic (F) and superconducting (S) signals. When the temperature of the system is decreased below $0.65T_c$ (~25 K), the S signals dominate over the F signals. The resulting magnetic hysteresis loops are highly asymmetric and the descending filed branch is nearly flat, as predicted in the case of surface pinning. At temperatures below $0.5T_c$ (~20 K), a sharp peak is developed near zero field in the magnetization hysteresis curves, implying an enhancement of superconducting vortex pinning. The observed pinning enhancement most likely results from magnetic pinning due to randomly distributed magnetic MgO grains, which yield the magnetic inhomogeneity and the related pinning potential in a length scale of ~100 nm. Thus, the present ferromagnetic/superconducting composite provides an ideal model system that demonstrates the availability of d^0 ferromagnetism as a source of magnetic potential for effective vortex pinning. © *2014 AIP Publishing LLC*. [http://dx.doi.org/10.1063/1.4865876]

I. INTRODUCTION

Bulk magnetic materials generally consist of multiple magnetic domains, which are groups of spins all pointing in the same direction and acting cooperatively. These magnetic domains are separated by narrow zone, typically ~10 to ~100 nm wide, of rapidly changing spin directions called domain walls. For magnetic materials of submicrometer size, however, the formation of domain walls is not necessarily energetically favored. At such small dimensions, comparable with the typical width of domain walls, properties of magnetic particles become complex. One example of complexity is a curling spin configuration, leading to a magnetization vortex state.[1–3] Much smaller grains (<~50 nm) show a stable single domain (SD) state. On further decrease in size, the SD state eventually transforms into a superparamagnetic state with zero coercivity and hysteresis. Thus, the magnetic structures of nanoscale systems are quite rich and versatile.[4,5]

Recently, magnetism in nanoscale materials has attracted additional attention since unexpected room-temperature ferromagnetisms has been observed in nanoscale oxides containing virtually no magnetic ions with partially-filled *d* or *f* shells, such as HfO_2, TiO_2, ZnO, MgO.[6–15] This so called d^0 ferromagnetism opened a new direction in the research field of dilute magnetic oxides and challenged the conventional paradigm of magnetism.[16,17] The true origin of d^0 ferromagnetism still remains to be clarified, but some surface and/or *grain-boundary related* defects are believed to play a leading role in the appearance of the long-range ferromagnetic ordering.[12–15]

Although it has not been recognized previously, d^0 ferromagnetism would also be interesting in terms of the interaction with the superconducting order. The influence of a ferromagnet (F) on an adjacent superconductor (S) is normally antagonistic; however, the nanoscale coexistence of different kinds of order parameters leads to intriguing phenomena, including fine-scale order parameter modulations,[18,19] triplet superconductivity,[20] and magnetic pinning,[21] as can be found in recent reviews.[22–25] Considering that d^0 ferromagnetism results from a mechanism that operates in nanocrystals, we expect that a d^0 ferromagnet/superconductor heterostructure exhibits an interesting, possibly constructive, interplay between F and S orders.

In this work, we hence investigate the magnetic properties of a d^0 ferromagnet/superconductor nanocomposite, in which MgO and MgB_2 phases are responsible for ferromagnetism and superconductivity, respectively. The magnetic properties of MgB_2/MgO composites have been investigated previously for the improvement of flux pinning.[26,27] In these composites, however, the MgO particles are considered to

a)Author to whom correspondence should be addressed. Electronic mail: uchino@kobe-u.ac.jp

behave simply as diamagnetic insulators to pin the vortex core, and the effect of ferromagnetism in MgO nanoparticles on the superconducting behavior of MgB_2 has not been investigated. We show that there exists an electromagnetic interaction between the vortex magnetic field and the stray field generated by the magnetic MgO nanoparticles in the present d^0 ferromagnet/superconductor nanocomposite, exhibiting magnetic pinning at temperatures below ~20 K. From the temperature dependence of the pinning behavior, we then discuss the size and spatial distribution of the magnetic particles dispersed in the composite.

II. EXPERIMENTAL PROCEDURES

The superconductor/d^0 ferromagnet composite was synthesized using solid phase reaction between pure Mg (99.9%) and B_2O_3 (99.9%). This method was originally developed by the present authors to synthesize highly luminescent and lasing MgO microcrystals.[28,29] The Mg/B_2O_3 mixture of molar ratio of 5:1 was thoroughly mixed and put in a cylindrical alumina crucible. This crucible was located inside a larger rectangular alumina crucible, which was closed with a 4-mm-thick alumina lid. This set of crucibles was placed in an electric furnace. The furnace was evacuated down to ~30 Pa before purging with argon. The Mg/B_2O_3 mixture was heated at desired temperatures (700 and 950 °C) for 3 h under flowing argon environment. After the heating process, some of the materials were sublimated and deposited outside the inner crucible, and the rest still remained in the bottom of the inner crucible. The deposited powder consists exclusively of MgO and exhibits efficient color-center-related photoluminescence emissions along with laser action.[29] On the other hand, the materials found in the inner crucible were black powder. This implies that B_2O_3 was reduced to B, yielding MgB_2 according to the following reaction:[29]

$$5Mg + B_2O_3 \rightarrow 3MgO + MgB_2 + Mg. \quad (1)$$

In this work, we will investigate the structural and magnetic properties of the black powder remained in the inner crucible. The samples prepared at 700 and 950 °C are referred to as S(700) and S(950), respectively.

Powder x-ray diffraction (XRD) patterns of the powdered sample were obtained with a diffractometer (Rigaku, SmartLab) using Cu K_α radiation. Scanning electron microscopy (SEM) and energy dispersive X-ray spectroscopy (EDS) were conducted with a scanning electron microscope (JEOL, JSM-5610LVS) with energy dispersive spectrometer. A commercial superconducting quantum interference device (SQUID) magnetometer (Quantum Design, MPMS-XL) equipped with the reciprocating sample option (RSO) was used for magnetic measurements. Magnetization M in a zero-field-cooled (ZFC) state was measured by cooling the sample initially in a zero field to 2 K, and the ZFC magnetization was recorded in an applied magnetic field H of 200 Oe as the temperature is increased. When the temperature reached ~300 K, the sample was gradually cooled under a magnetic field of 200 Oe to obtain the field-cooled (FC) magnetization. The $M(H)$ curves were measured at different temperatures after zero-field cooling without correcting for the diamagnetic background.

III. RESULTS

A. Structural characterization

A representative XRD pattern, a SEM image, and EDS element mapping data measured for S(700) are shown in Fig. 1. From the θ-2θ XRD pattern, one sees that the resulting composite consists of Mg, MgO, and MgB_2, as inferred from Eq. (1). From the full-width at half-maximum (FWHM) of the MgO (220) peak at an angle of $2\theta = \sim 62°$ and the Scherrer formula, we estimated that the primary crystallite size of MgO is in the range 17 ± 3 nm. On the other hand, the primary crystallite size of MgB_2 is difficult to be evaluated correctly because of the relatively low Bragg peak intensities. The SEM image [Fig. 1(b)] and the corresponding EDS element mapping data [Figs. 1(c)–1(e)] demonstrate that the constituent crystalline materials are not phase separated at least on the length scale of several micrometers but rather form a textured homogeneous composite.

As for S(950), we found that the product consists only of MgB_2 and MgO [see the upper curve in Fig. 1(a)]. This indicates that the unreacted Mg metal was further oxidized at 950 °C by the residual oxygen remained in the furnace. It should also be noted that the FWHM of the diffraction peaks attributed to MgO becomes smaller when the reaction was conducted at 950 °C. Accordingly, the Scherrer formula predicts a larger crystallite size (~40 nm) for the MgO crystals in S(950) than that of the MgO crystals in S(700).

B. Magnetic properties

Figure 2 compares the room-temperature ($T = 300$ K) magnetization (M) versus magnetic field (H) curves of S(700) and S(950). One sees from Fig. 2 that both of the samples demonstrate a ferromagnetic hysteresis behavior. However, the saturation magnetization and remanence of S(700) are much larger (an order of magnitude or more) than those of S(950). The relative remanence (remanent magnetization M_r/saturation magnetization M_s) and the coercive field H_c of S(700) are 19% and 120 Oe, respectively. In spite of the extensive researches on MgB_2 thin films and nanoparticles, ferromagnetisms have not been reported and recognized previously in any of the MgB_2 nanostructures,[30,31] to the best of our knowledge. We hence suggest that the observed ferromagnetism results from the nanocrystalline MgO phase, as has often been reported previously.[8,13] The enhanced ferromagnetic characteristics in S(700) imply that smaller or more defective MgO crystals are responsible for the appearance of the ferromagnetic order. In what follows, we will hence mainly investigate the magnetic properties of S(700).

The ferromagnetic behavior of S(700) can also be recognized in temperature dependent irreversibility of the ZFC and FC curves measured with an applied magnetic field of $H = 200$ Oe (see Fig. 3). The splitting of the ZFC and FC curves is clearly visible in the temperature region from

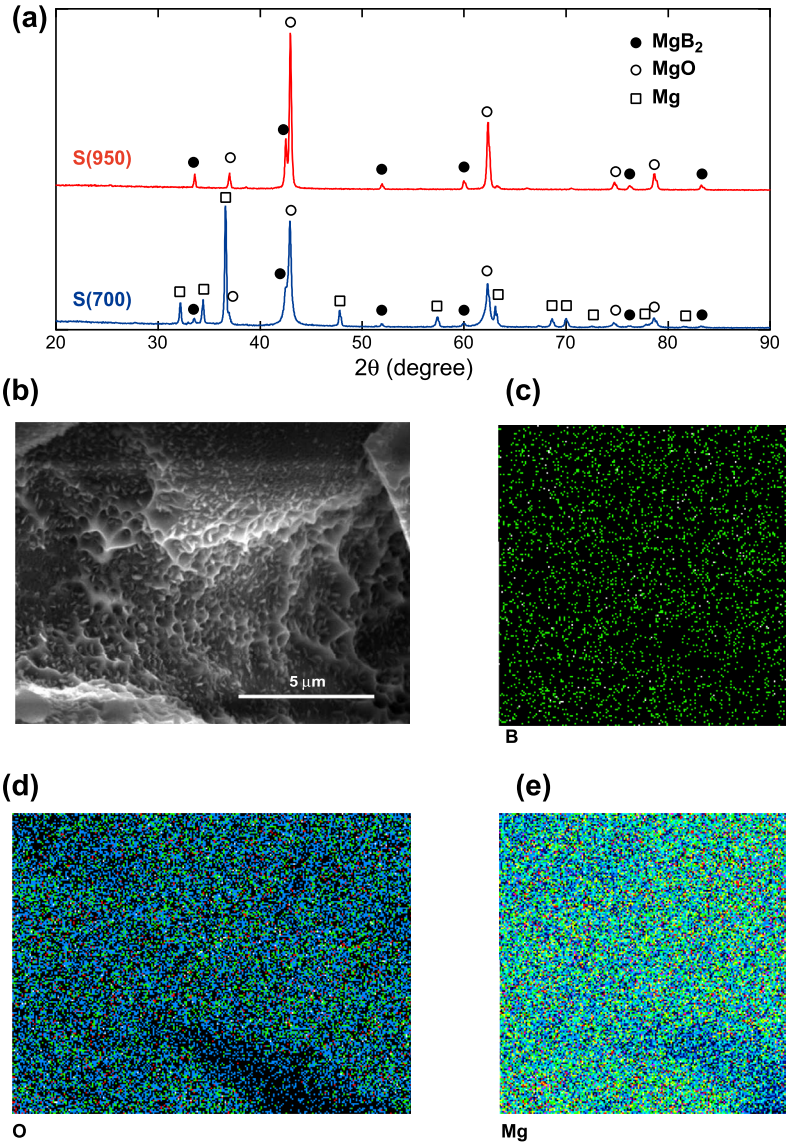

FIG. 1. (a) X-ray diffraction pattern of S(700) (lower pattern) and S(950) (upper pattern). (b) A representative SEM image of S(700). SEM-EDS element mapping data of (c) B, (d) O, and (e) Mg elements throughout the region shown in (b).

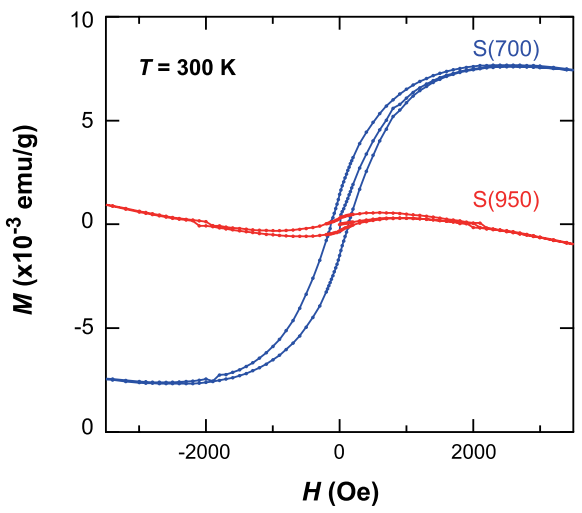

FIG. 2. Magnetic-field (H) dependence of magnetization (M) of S(700) and S(950) measured at $T = 300$ K.

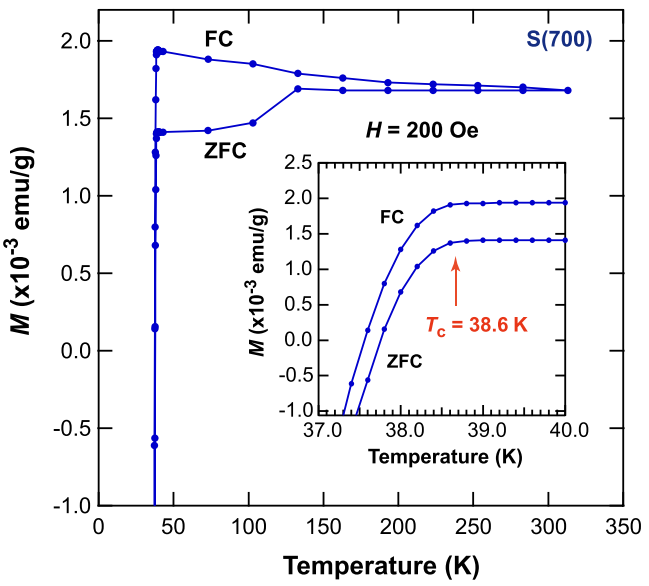

FIG. 3. ZFC and FC $M(T)$ curves of S(700) measured under applied field of 200 Oe. The inset shows a magnified plot of the ZFC and FC curves in temperature region from 37 to 40 K.

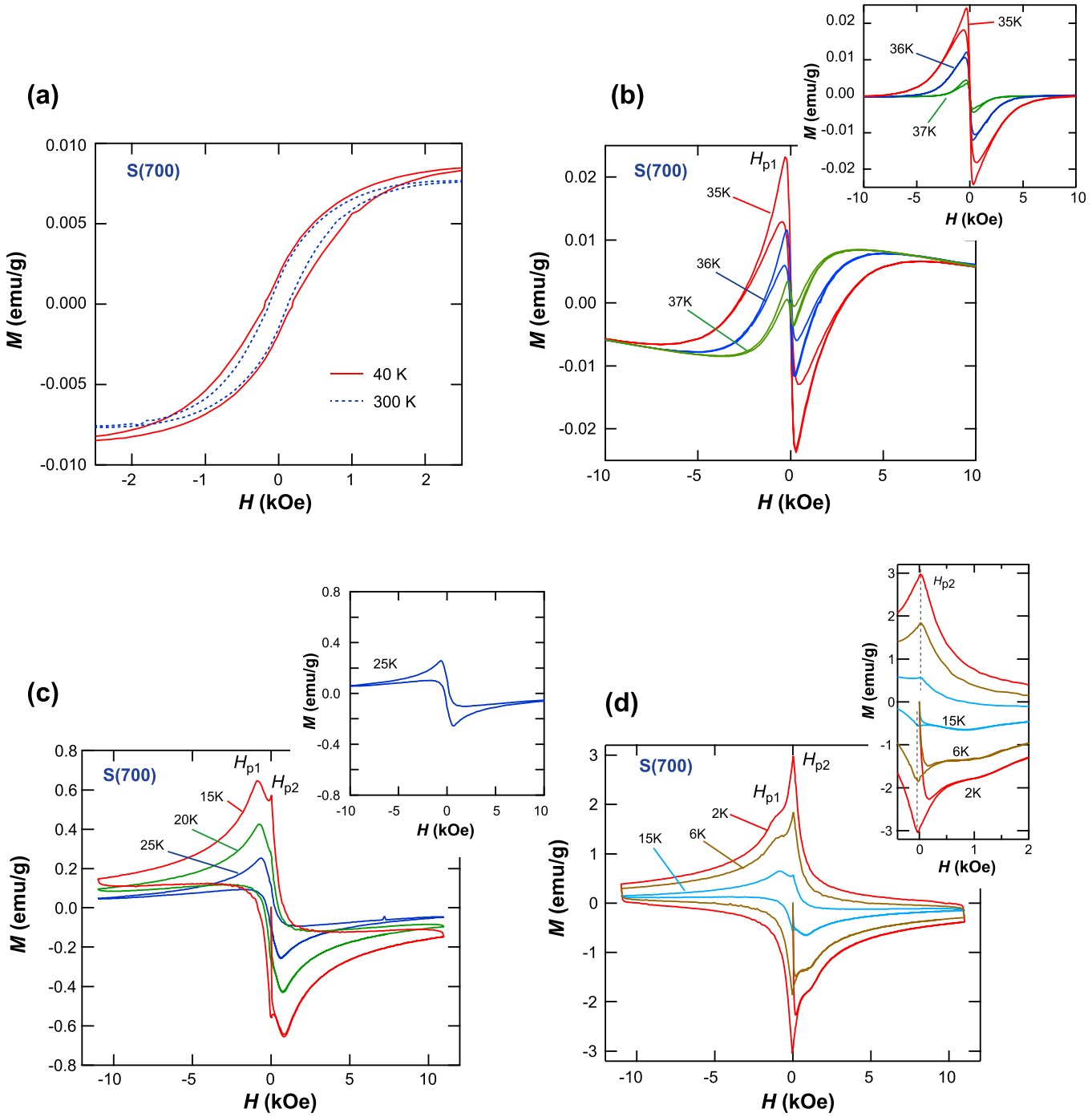

FIG. 4. Magnetic-field (H) dependence of magnetization (M) of S(700) measured at (a) $T = 40$ and 300 K, (b) $T = 35$, 36, and 37 K, (c) $T = 15$, 20, and 25 K and (d) $T = 2$, 6, and 15 K. H_{p1} indicates a temperature-dependent peak field, whereas H_{p2} designates a temperature-independent peak field occurring near zero field. The insets in (b) and (c) show the $M(H)$ curves after subtracting the magnetization at $T = 40$ K. The inset in (d) shows a magnified plot in the magnetic field region from −500 to 2000 Oe.

~40 to ~300 K, in agreement with the room-temperature ferromagnetic hysteresis behavior shown in Fig. 2. It should also be noted that the ZFC/FC curves exhibit a sharp drop in M starting at 38.6 K and eventually become negative at lower temperatures ($T < \sim 37.5$ K) (see the inset of Fig. 3). This observed signature of the diamagnetic response indicates that the critical superconducting transition temperature T_c is ~ 39 K. The observed T_c value is almost equal to the one reported for a pure MgB_2 crystal ($T_c = 39$ K).[32]

We next investigate the temperature dependence of the $M(H)$ curves. Although, the relative remanence and coercivity are slightly increased with decreasing temperature [$M_r/M_s = 21\%$ and $H_c = 180$ Oe at $T = 40$ K, see Fig. 4(a)], the shape of the hysteresis loop remains basically unchanged in the 300-40 K region. Upon cooling below T_c to 35 K, one sees a superposition of the F and S signals, yielding a broad negative peak H_{p1} on the descending branch of the $M(H)$ curves [see Fig. 4(b)]. To eliminate the contribution of the F signals from these $M(H)$ curves, we subtracted the $M(H)$ data

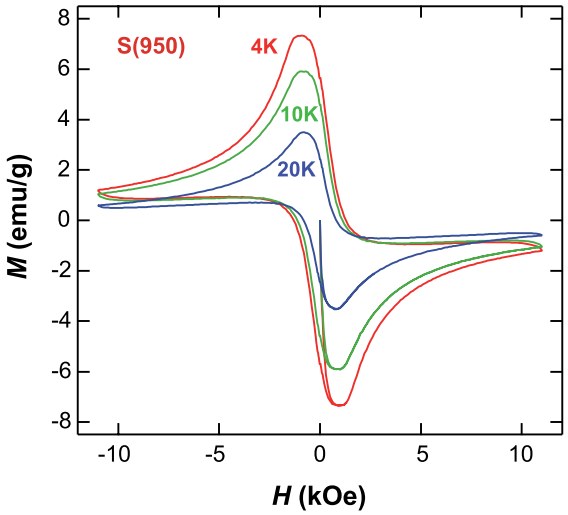

FIG. 5. $M(H)$ curves of S(950) measured in the temperature region from 4 to 20 K.

at $T = 40$ K, as shown in the inset of Fig. 4(b). The resulting difference $M(H)$ curves exhibit a very small hysteresis. This indicates that the $M(H)$ dependence is quite reversible in the near T_c region. Such a reversible $M(H)$ dependence is expected to occur in a superconducting crystal or grains in a polycrystalline sample with a size smaller than 2λ, where λ is the magnetization penetration depth.[33] In the temperature region higher than 35 K, the value of λ in MgB_2 has been estimated to be ~250 nm or more.[34] Thus, the size of the present MgB_2 crystallites is considered to be on the order of ~500 nm.

In the temperature region below ~25 K, the S signals begin to dominate over the F signals [see Fig. 4(c)]. We should note that the shape of the $M(H)$ curve at 25 K is almost unchanged even if the magnetization at $T = 40$ K is subtracted, as shown in the inset of Fig. 4(c). This indicates that the sample's magnetization is determined mostly by the magnetic response of the superconducting phase. Figure 4(c) also shows that the moment on the decreasing (increasing) field cycle in the positive (negative) field is almost parallel to the field axis. Such an asymmetric $M(H)$ hysteresis loop is commonly observed in the powder samples where the magnetic moment is determined by geometrical and Bean-Livingston surface barriers.[35,36] The value of λ in bulk MgB_2 is estimated to be ~70–~100 nm in the temperature range of ~10–~25 K,[34] and hence 2λ becomes comparable with or smaller than the size of the MgB_2 crystallites. Accordingly, surface pinning begins to operate in the composite in this temperature region.

One also notices from Fig. 4(c) that at temperatures below ~20 K, a rather sharp peak, designated as H_{p2}, emerges on the higher filed side of H_{p1} on the descending field branch of the loop. When the sample is cooled further, down to 2 K, H_{p2} shows a substantial increase in intensity. It should be noted that the position of H_{p2} is almost temperature independent and resides at a slightly positive field ($H \sim 40$ Oe) on the descending field branch [see the inset of Fig. 4(d)]. Such a double peak feature, especially the central positive peak feature H_{p2}, has not been observed previously in the $M(H)$ loops of MgB_2 powders and/or thin films[26,31,37,38] nor in those of S(950), as shown in Fig. 5. This allows us to assume that the pinning force relevant to H_{p2} results from a certain magnetic interaction between ferromagnetic and superconducting states, as will be discussed in Sec. IV A in more detail.

IV. DISCUSSION

A. Origin of H_{p2} and its relation to magnetic pinning

As shown in Fig. 4, the most notable feature found in the $M(H)$ loops of S(700) is the development the sharp peak (H_{p2}) near zero field at temperatures below ~20 K. Note also that the position of H_{p2} is almost temperature independent and is located on the positive (negative) side on the descending (ascending) branch of the loop. According to the critical state model, a central peak in the $M(H)$ loop shifts to the negative (positive) side on the descending (ascending) field branch, as in the case of H_{p1};[39] the shift normally results from the local flux density, lagging behind the applied field. Thus, the development of H_{p2} cannot be simply interpreted in terms of the conventional demagnetization scheme.

Previously, it has been demonstrated that granular superconductors show a positive central peak in the $M(H)$ loop on the descending field branch.[40–42] Granularity in superconductors induces demagnetization fields which strongly modify the intergranular currents,[40–42] even inducing a shift of the central peak in the positive direction on the descending field branch. In these granular superconductors, however, the positive shift of the central peak becomes more pronounced with decreasing temperature. Furthermore, the central peak of granular superconductors becomes quite broad with decreasing temperature well below T_c.[40–42] These temperature dependent behaviors contrast with those of H_{p2}, as shown in Fig. 4. We hence consider that the present positive central peak feature H_{p2} does not result from the grain-induced demagnetization effect.

A positive central peak on the descending field branch has also been observed from some S/F heterostructures with magnetic pinning.[43–45] Magnetic pinning arises from the electromagnetic interaction between the superconducting vortices and the stray field generated by the magnetic texture in the vicinity of the superconductor surface.[21] The resulting $M(H)$ loops become highly asymmetric to the $M = 0$ axis and only symmetric with respect to the origin,[43–45] in agreement with the magnetic hysteretic behavior shown in Fig. 4. This indicates that the magnetization at a fixed external field is affected by the direction of the field sweep, which is different from vortex core pinning by non-magnetic pinning centers. It should also be noted that H_{p2} is not observed in the $M(H)$ loops of S(950) but exclusively found in those of S(700), as noted earlier. It is hence reasonable to assume that the positive central peak H_{p2} results from the magnetic pinning due to the expected electromagnetic response in the present F/S composite.

To realize the magnetic pinning in S/F structures, one has to create spatial modulation of the local magnetic field on the length scale of λ by using, for example, regular arrays of ferromagnetic dots or rods in the vicinity of S layers, or

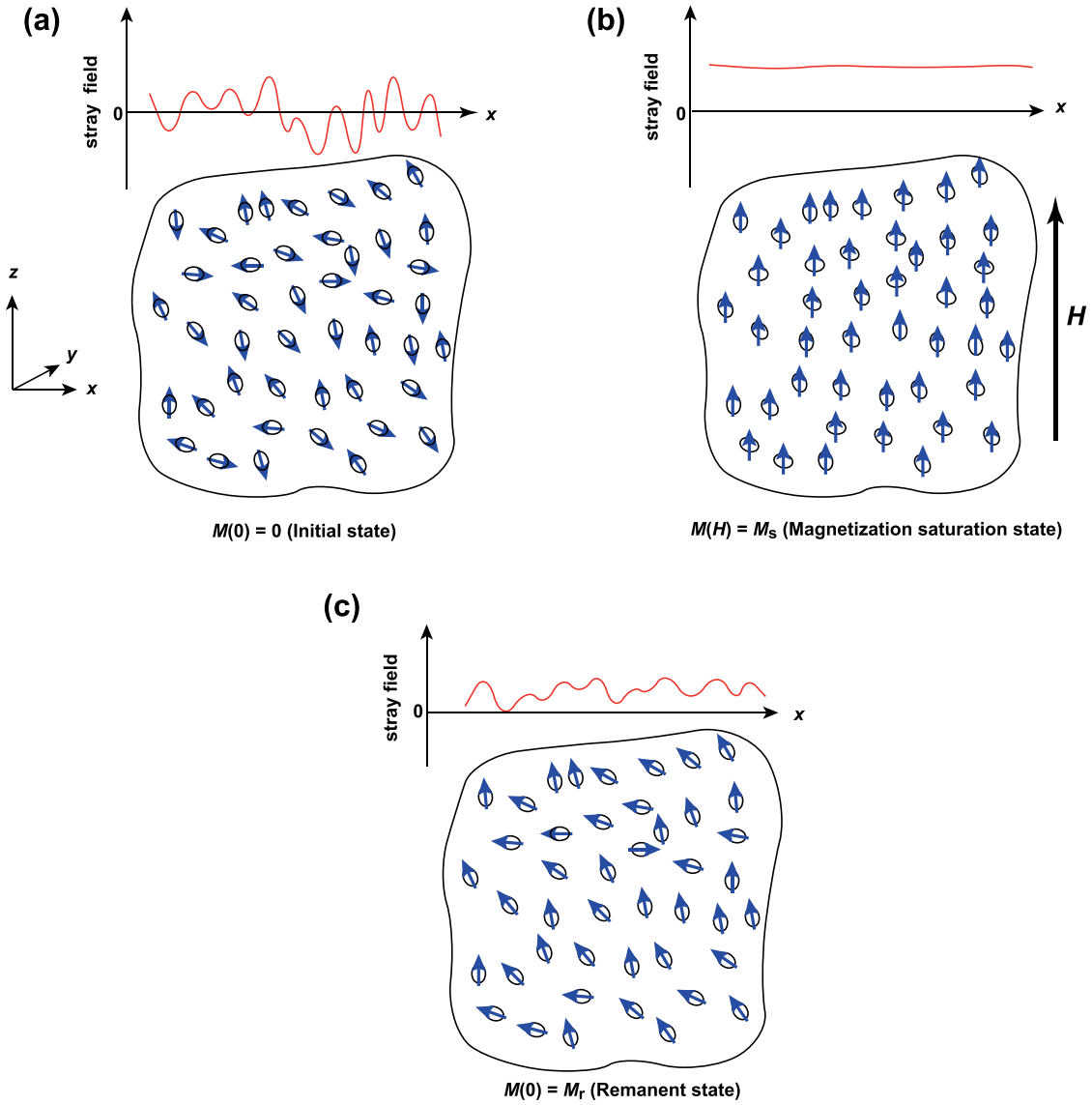

FIG. 6. Schematic representations of magnetization directions within the assumed single-domain grains (lower) and the corresponding z-component of stray field vs lateral distance x (upper). Ellipses symbolically represent uniaxially anisotropic single-domain grains, in which the easy axis is directed along the major axis of each ellipse. The arrow on each ellipse indicates direction of the magnetization vector. (a) The initial $H = 0$ state. (b) The saturation magnetization state in which the magnetization vector of every grain is aligned with the applied field $\boldsymbol{H}$. (c) The remanent magnetization state, which is obtained after removing the applied field in (b).

intrinsic magnetic domains, such as stripe domains, within F layers.[21,23,43–46] Furthermore, F and S structures must be electronically decoupled by an appropriate buffer layer to avoid proximity effect.[21] Thus, the elaborate design and fabrication of the F/S structures are required for the realization of efficient magnetic pinning, which is still an ongoing research challenge.[47–49]

In our F/S composite, the above conditions to realize magnetic pinning are likely to be satisfied intrinsically. The F regions with near zero remanence are expected to have nanoscale magnetic inhomogeneities. These intrinsic magnetic inhomogeneities will be almost frozen below H_c ($\sim$200 Oe), hence creating magnetic gradients and the resulting pinning potentials. Provided that ferromagnetic particles are randomly distributed in the composite, this disorder yields the magnetic gradients for any orientation of the system. In addition, not all of the MgO nanocrystals in the composite will show ferromagnetism, but some of them will behave as insulating buffer layers to avoid the direct interaction between S and F orders.

Considering that the magnetic pinning acts on a length scale comparable with the penetration depth, we can roughly estimate the extent of the magnetic inhomogeneity in the composite. As shown in Fig. 4, H_{p2} tends to emerge at temperatures $T < \sim$20 K. In this temperature region, it has been estimated, as mentioned previously in this paper, that the value of λ in MgB_2 is an order of 100 nm or less, whereas it shows an abrupt increase to $\sim$200 nm or more for temperatures above 25 K.[34] This allows us to expect that the length scale of the magnetic inhomogeneity is on the order of 100 nm, which is several times larger than the estimated (or averaged) size of the primary MgO crystallites ($\sim$20 nm) in the composite. This implies that the expected magnetic gradients are derived not from the individual primary MgO

crystallites but from a certain collective effect of, for example, their aggregates with larger dimensions.

B. Model of the formation of magnetic potentials

On the basis of the considerations given in Sec. IV A, we will give a schematic model of the formation of magnetic potentials in the present F/S composite. A likely scenario is that magnetic aggregates with a size of ~100 nm are embedded and randomly dispersed in the insulating matrix so that the effective pinning potentials are created in the composite. As a zeroth-order approximation, we first assume that all the magnetic aggregates in the composite are considered as noninteracting SD grains with uniform $\boldsymbol{M}_s$, where $\boldsymbol{M}_s$ indicates the saturation magnetization vector, because of the size effect of magnetic nanoparticles. It would also be reasonable to expect that the grain possesses shape and/or magnetocrystalline anisotropy. For simplicity, we assume that only one preferred direction for $\boldsymbol{M}_s$, or uniaxial anisotropy, is present within the individual SD grains.

If the sample has not previously been exposed to a magnetic field vector $\boldsymbol{H}$, the net magnetization of the sample is 0 because $\boldsymbol{M}_s$ of the individual SD grains is randomly directed [see Fig. 6(a)]. This magnetic inhomogeneity will create a gradient in magnetic field within a certain local region [see also Fig. 6(a)]. As the field is applied, $\boldsymbol{M}_s$ of each SD grain begins to rotate toward the direction of $\boldsymbol{H}$. If the applied field is increased to a sufficient level, all grains will have $\boldsymbol{M}_s$ aligned with the direction of $\boldsymbol{H}$ [see Fig. 6(b)]. This magnetization saturation state will not form a field gradient even within a local region, creating an almost flat potential [see also Fig. 6(b)]. During removal of the magnetic field, $\boldsymbol{M}_s$ of individual SD grains rotates to the nearest energetically preferred direction of the grains. Accordingly, the magnetic inhomogeneity begins to reemerge. After complete removal of the magnetic field, or $\boldsymbol{H}=0$, a remanent magnetization, M_r, will remain. As for an assembly of uniaxial SD grains that have isotropic random orientations of their easy axes, the relative remanence M_r/M_s is estimated to be 0.5,[50] which is much larger than the one observed in S(700) [$M_r/M_s=0.21$ at 40 K, see Fig. 4(a)]. This discrepancy most likely results from the oversimplification of the assumed model. The real system may contain, for example, a large percentage of multidomain grains, which can substantially lower the remanent magnetization. The observed low relative remanence allows us to expect that the magnetic state of the present composite is highly inhomogeneous as long as the applied field is close to zero. Accordingly, the local magnetic field will be highly spatially modulated in the near-zero field region, creating local magnetic gradients similar to the initial magnetic state shown in Fig. 6(a).

The pinning potential thus created is, in principle, temperature independent. For effective magnetic pinning, however, the penetration depth must become comparable with the spatial extent of the magnetic potential, as mentioned repeatedly in this work. The above conditions are likely to be fulfilled at temperatures below ~20 K, whereupon effective magnetic pinning tends to occur, resulting in H_{p2} in the $M(H)$ curves.

V. CONCLUSIONS

We have investigated the magnetic properties of the F/S composite prepared by solid phase reaction between Mg and B_2O_3 under Ar atmosphere. When the reaction was conducted at 700 °C, the composite consisting of MgO, MgB_2, and unreacted Mg were obtained. The composite exhibits a ferromagnetic hysteresis behavior in the temperature region from 300 to 40 K. The relative remanence and the coercive field at 300 K (40 K) are 19% (21%) and 120 Oe (180 Oe), respectively. Defective MgO nanocrystals (~20 nm) embedded in the composite are most likely responsible for the observed ferromagnetism. The superconducting transition with the onset temperature of 38.6 K was recognized by the ZFC and FC magnetization curves, indicating that the defect-induced ferromagnetic order in the composite does not lower T_c of the MgB_2 phase. At temperatures well below T_c ($T<\sim20$ K), a positive central peak H_{p2} was found to develop on the descending field branch of the $M(H)$ loop. The appearance of H_{p2} can be interpreted in terms of the magnetic pinning associated with the inhomogeneous magnetic structures realized in the composite. On the basis of these observations, we suggest that the present F/S composite can be regarded as a nanoscale assembly of F and S grains, which are finely dispersed randomly at the ~100 nm scale in an insulating matrix so that it ensures effective magnetic pinning. Thus, we can conclude that nanoscale oxides with d^0 ferromagnetic order will serve as an ideal counterpart to superconductors in terms of magnetic pinning of vortices.

[1]T. Shinjo, T. Okuno, R. Hassdorf, K. Shigeto, and T. Ono, Science **289**, 930 (2000).
[2]A. Wachiwiak, J. Wiebe, M. Bode, O. Pietzsch, M. Morgenstern, and R. Wiesendanger, Science **298**, 577 (2002).
[3]H. F. Ding, A. K. Schmid, D. Li, K. Yu. Guslienko, and S. D. Bader, Phys. Rev. Lett. **94**, 157202 (2005).
[4]Y. Li, P. Xiong, S. von Molnár, Y. Ohno, and H. Ohno, Phys. Rev. B **71**, 214425 (2005).
[5]R. K. Dumas, C.-P. Li, I. Roshchin, I. K. Schuller, and K. Liu, Phys. Rev. B **75**, 134405 (2007).
[6]V. M. Venkatesan, C. B. Fitzgerald, and J. M. D. Coey, Nature **430**, 630 (2004).
[7]A. Zunger, S. Lany, and H. Raebiger, Physics **3**, 53 (2010).
[8]M. Stoneham, J. Phys.: Condens. Matter **22**, 074211 (2010).
[9]R. Oja, M. Tyunina, L. Yao, T. Pinomaa, T. Kocourek, A. Dejneka, O. Stupakov, M. Jelinek, V. Trepakov, S. van Dijken, and R. M. Nieminen, Phys. Rev. Lett. **109**, 127207 (2012).
[10]N. H. Hong, J. Sakai, N. Poirot, and V. Brizé, Phys. Rev. B **73**, 132404 (2006).
[11]A. Sundaresan, R. Bhagavi, N. Rangarajan, U. Siddesh, and C. N. R. Rao, Phys. Rev. B **74**, 161306(R) (2006).
[12]B. B. Straumal, A. A. Mazilkin, S. G. Protasova, A. A. Myatiev, P. B. Straumal, G. Schütz, P. A. van Aken, E. Goering, and B. Baretzky, Phys. Rev. B **79**, 205206 (2009).
[13]C. Martínez-Boubeta, J. I. Beltrán, L. Balcells, Z. Konstantinović, S. Valencia, D. Schmitz, J. Arbiol, S. Estrade, J. Cornil, and B. Martínez, Phys. Rev. B **82**, 024405 (2010).
[14]F. Wang, Z. Pang, L. Lin, S. Fang, Y. Dai, and S. Han, Phys. Rev. B **80**, 144424 (2009).
[15]T. Uchino and T. Yoko, Phys. Rev. B **85**, 012407 (2012).
[16]J. D. M. Coey, Curr. Opin. Solid State Mater. Sci. **10**, 83 (2006).
[17]T. Dietl, Nature Mater. **9**, 965 (2010).
[18]P. Fulde and R. A. Farrel, Phys. Rev. **135**, A550 (1964).
[19]A. I. Larkin and Y. N. Ovchinnikov, Sov. Phys. JETP **20**, 762 (1965).
[20]S. S. Saxena, P. Agarwal, K. Ahilan, F. M. Grosche, R. K. W. Haselwimmer, M. J. Steiner, E. Pugh, I. R. Walker, S. R. Julian, P.

Monthoux, G. G. Lonzarich, A. Huxley, I. Sheikin, D. Braithwaite, and J. Flouquet, Nature **406**, 587 (2000).
[21]L. N. Bulaevskii, E. M. Chudnovsky, and M. P. Maley, Appl. Phys. Lett. **76**, 2594 (2000).
[22]A. I. Buzdin, Rev. Mod. Phys. **77**, 935 (2005).
[23]I. F. Lyuksyutov and V. L. Pokrovsky, Adv. Phys. **54**, 67 (2005).
[24]F. S. Bergeret, A. F. Volkov, and K. B. Efetov, Rev. Mod. Phys. **77**, 1321 (2005).
[25]A. Yu. Aladyshkin, A. V. Silhanek, W. Gillijns, and V. V. Moshchalkov, Supercond. Sci. Technol. **22**, 053001 (2009).
[26]C. B. Eom, M. K. Lee, J. H. Choi, L. J. Belenky, X. Song, L. D. Cooley, M. T. Naus, S. Patnaik, J. Jiang, M. Rikel, A. Polyanskii, A. Gurevich, X. Y. Cai, S. D. Bu, S. E. Babcock, E. E. Hellstrom, D. C. Larbalestier, N. Rogado, K. A. Regan, M. A. Hayward, T. He, J. S. Slusky, K. Inumaru, M. K. Haas, and R. J. Cava, Nature **411**, 558 (2001).
[27]Y. B. Zhang, D. F. Zhou, Z. X. Lv, Z. Y. Deng, C. B. Cai, and S. P. Zhou, J. Appl. Phys. **107**, 123907 (2010).
[28]T. Uchino and D. Okutsu, Phys. Rev. Lett. **101**, 117401 (2008).
[29]Y. Uenaka and T. Uchino, Phys. Rev. B **83**, 195108 (2011).
[30]A. Gümbel, J. Eckert, G. Fuchs, K. Nenkov, K.-H. Müller, and L. Schultz, Appl. Phys. Lett. **80**, 2725 (2002).
[31]X. X. Xi, Supercond. Sci. Technol. **22**, 043001 (2009).
[32]J. Nagamatsu, N. Nakagawa, T. Muranaka, Y. Zenitani, and J. Akimitsu, Nature **410**, 63 (2001).
[33]D. M. Gokhfeld, D. A. Balaev, M. I. Petrov, S. I. Popkov, K. A. Shaykhutdinov, and V. V. Val'kov, J. Appl. Phys. **109**, 033904 (2011).
[34]B. Kang, H.-J. Kim, M.-S. Park, K.-H. Kim, and S.-I. Lee, Phys. Rev. B **69**, 144514 (2004).
[35]C. P. Bean and J. D. Livingston, Phys. Rev. Lett. **12**, 14 (1964).
[36]C. D. Dewhurst, D. A. Cardwell, A. M. Campbell, R. A. Doyle, G. Balakrishnan, and D. McK Paul, Phys. Rev. B **53**, 14594 (1996).
[37]M. Pissas, E. Moraitakis, D. Stamopoulos, G. Papavassiliou, V. Psycharis, and S. Koutandos, J. Supercond. **14**, 615 (2001).
[38]X. H. Zeng, A. Sukiasyan, X. X. Xi, Y. F. Hu, E. Wertz, Qi Li, W. Tian, H. P. Sun, X. Q. Pan, J. Lettieri, D. G. Schlom, C. O. Brubaker, Zi-Kui Liu, and Qiang Li, Appl. Phys. Lett. **79**, 1840 (2001).
[39]T. H. Johansen and H. Bratsberg, J. Appl. Phys. **77**, 3945 (1995).
[40]D. V. Shantsev, M. R. Koblischka, Y. M. Galperin, T. H. Johansen, L. Půst, and M. Jirsa, Phys. Rev. Lett. **82**, 2947 (1999).
[41]M. R. Koblischka, L. Půst, A. Galkin, and P. Nálevka, Appl. Phys. Lett. **70**, 514 (1997)
[42]J. Horvat, S. Soltanian, A. V. Pan, and X. L. Wang, J. Appl. Phys. **96**, 4342 (2004).
[43]S. Kobayashi, H. Oike, M. Takeda, and F. Itoh, Phys. Rev. B **66**, 214520 (2002).
[44]J. Albrecht, S. Soltan, and H.-U. Habermeier, Phys. Rev. B **72**, 092502 (2005).
[45]M. Z. Cieplak, L. Y. Zhu, Z. Adamus, M. Kończykowski, and C. L. Chien, Phys. Rev. B **84**, 020514(R) (2011).
[46]D. B. Jan, J. Y. Coulter, M. E. Hawley, L. N. Bulaevskii, M. P. Maley, Q. X. Jia, B. B. Maranville, F. Hellman, and X. Q. Pan, Appl. Phys. Lett. **82**, 778 (2003).
[47]V. Vlasko-Vlasov, A. Buzdin, A. Melnikov, U. Welp, D. Rosenmann, L. Uspenskaya, V. Fratello, and W. Kwok, Phys. Rev. B **85**, 064505 (2012).
[48]J. E. Villegas, C.-P. Li, and I. K. Schuller, Phys. Rev. Lett. **99**, 227001 (2007).
[49]T. Petrisor, Jr., M. S. Gabor, C. Tiusan, V. Galluzzi, G. Celentano, S. Popa, A. Boulle, and T. Petrisor, J. Appl. Phys. **112**, 053919 (2012).
[50]E. C. Stoner and E. P. Wohlfarth, Philos. Trans. R. Soc. London, Ser. A **240**, 599 (1948).